Optics & Laser Technology 44 (2012) 2186–2196

Contents lists available at SciVerse ScienceDirect

Optics & Laser Technology

journal homepage: www.elsevier.com/locate/optlastec

Real-time monitoring of laser welding of galvanized high strength steel in lap joint configuration

Fanrong Kong [a], Junjie Ma [a], Blair Carlson [b], Radovan Kovacevic [a,*]

[a] Center for Laser-aided Manufacturing, Southern Methodist University, 3101 Dyer Street, Dallas, TX 75205, USA
[b] General Motors R&D Center, Warren, MI 48090-9055, USA

ARTICLE INFO

Article history:
Received 3 November 2011
Received in revised form
9 February 2012
Accepted 3 March 2012
Available online 28 March 2012

Keywords:
Laser welding
Galvanized steel
Plasma spectroscopy

ABSTRACT

Two different cases regarding the zinc coating at the lap joint faying surface are selected for studying the influence of zinc vapor on the keyhole dynamics of the weld pool and the final welding quality. One case has the zinc coating fully removed at the faying surface; while the other case retains the zinc coating on the faying surface. It is found that removal of the zinc coating at the faying surface produces a significantly better weld quality as exemplified by a lack of spatters whereas intense spatters are present when the zinc coating is present at the faying surface. Spectroscopy is used to detect the optical spectra emitted from a laser generated plasma plume during the laser welding of galvanized high strength DP980 steel in a lap-joint configuration. A correlation between the electron temperature and defects within the weld bead is identified by using the Boltzmann plot method. The laser weld pool keyhole dynamic behavior affected by a high-pressure zinc vapor generated at the faying surface of galvanized steel lap-joint is monitored in real-time by a high speed charge-coupled device (CCD) camera assisted with a green laser as an illumination source.

1. Introduction

Laser welding of galvanized steel in lap joint configuration is one of the most challenging issues in the welding community because the presence of highly pressurized zinc vapor can easily disturb the stability of liquid flow in the weld pool resulting in poor weld quality. Some experimental approaches have been undertaken to resolve the zinc vapor problem in the welding of galvanized steels in lap joint configuration, for example, removing the zinc at the faying surface [1], presetting aluminum [2] or copper foil [3] along the faying surface, adopting dual beam laser [4], introducing arc to preheat the galvanized steel coupon [5], etc. In order to guarantee the weld quality of galvanized steel joints, real-time detection of the weld defects could be indirectly achieved by monitoring a number of different signals during the welding process, such as emissivity of light, sound, image of the molten pool, etc.

The interaction between the laser beam and metal is often related with the ejection of material in the liquid and gaseous states from the molten pool in the high power laser beam welding process. The ejected metal usually consists of excited ions and atoms, which is referred to as a plume [6]. The material under the laser radiation will be rapidly heated to a temperature exceeding the boiling point accompanied by the formation of plasma. Considering that the plasma is generated only when vaporization occurs, its presence is related to a minimum temperature and specific event such that it may provide useful information about the welding conditions. Some light signals coming from the plasma may be utilized to achieve information regarding the possible presence of defects during the process. Fabbro et al. [7] studied both the keyhole dynamic and the trajectories of the escaping zinc vapor at the interface of two steel sheets across the keyhole both numerically and experimentally. However, neither qualitative nor quantitative detection of the zinc above the top sheet or under the bottom sheet was achieved in their experiments, which is a severe limitation for application to an industrially relevant condition. Park et al. [8] experimentally monitored the CO_2 laser welding by a photodiode-based acquisition of the ultraviolet (UV) emission from the plasma zone and the infrared radiation (IR) from the weld pool and spatter. By this means authors studied the relationship between welding conditions including laser power, welding speed and nozzle position and the spectral line intensities from the plasma emission together with IR emission from the weld pool. However, the limitation of this method is difficult to separate the IR emission related to the weld pool from the IR emission related to the plasma zone [6]. Park and Rhee [9] experimentally studied the welding mechanism as well as weld defects such as spattering during CO_2 laser welding of galvanized steel, in which a bead-on-plate configuration was chosen without

* Corresponding author. Tel.: +1 214 768 4865; fax: +1 214 768 2116.
E-mail address: kovacevi@lyle.smu.edu (R. Kovacevic).

0030-3992/$ - see front matter © 2012 Elsevier Ltd. All rights reserved.
http://dx.doi.org/10.1016/j.optlastec.2012.03.003

any problem of zinc vapor worsening the weld quality. In addition, Bruncko et al. [10] experimentally monitored the influence of focal position of the laser beam on the featured emission line intensities detected from the laser induced plasma by using optical emission spectroscopy in the bead-on-plate welding by laser for an austenitic steel sheet. Rodil et al. [11] monitored the laser welding quality in a bead-on-plate weld by using spectroscopy and studied the correlations between the power spectrum and the weld defects. In addition, Mirapeix et al. [12], Ancona et al. [13], Sadek et al. [14], Kato et al. [15], Li et al. [16], and Allende et al. [17] separately applied spectroscopy to study the correlations between the emission line intensities of selected elements detected from arc plasma and penetration depth of the weld and welding defects like blowhole and pores retained in the weld. However, there were limited literature which can be found studying the correlations between the featured optical spectrum and zinc vapor induced spatters in the laser welding of galvanized steel for an overlap joint configuration. Considering the importance of welding of galvanized steel applied into the automobile industry, it will be very meaningful to real-time monitor the welding quality by detecting the featured change of emission line intensities in the welding of galvanized steel.

In this study, we are expecting that spectrographic monitoring of the laser weld pool and associated plasma zone has the potential to be utilized as a feedback for process control to enable defect-free welds. The Boltzmann-plot method is introduced to calculate the electron temperature of laser induced plasma by selected zinc and iron elements in the overlapped galvanized steel weld. A series of experiments is also performed to study the influence of welding parameters on the weld quality in the laser welding of galvanized high-strength steel in a lap joint configuration, in which a high speed CCD camera with a green laser as an illumination source and a spectroscopic monitoring system are used to study weld defects by monitoring weld pool dynamics and emission lines from the laser induced plasma zone, respectively.

2. Experimental setup and procedure

Experiments are carried out using a 4 kW fiber laser (see Fig. 1). The welding head has a 150 mm focal distance, which generates a 0.6 mm focal spot. Pure argon is used as a shielding gas at a typical flow rate of 35 standard cubic feet per hour (SCFH). The coupons of galvanized steel are 1.2 mm and 1.5 mm in thickness, with a 10 μm thick zinc coating on the top and bottom surfaces. A zero gap in the lap joint configuration is assured by using a controlled clamping force. The surface quality of the weld seam is verified by an optical microscope. Finally, in order to visualize the dynamics of the molten pool, a CCD camera, with a frame rate of 4000 frames per second is used. The spectrometer is set above the coupons at a distance of 200 mm from the weld pool and fixed to the robotic arc together with the laser head (see Fig. 1). An Ocean Optics spectrometer (SD2000) was used to detect the elemental composition in the laser induced plasma. The integration time is 3 ms, the wavelength resolution is 0.364 nm, and the slit width is 50 μm. First, the chemical composition referenced in literature [18,19] was input into the analysis software of spectrometer as known condition. Then the featured emission lines are linked to the chemical elements by using the corresponding software of the spectrometer. Among all of the chemical elements, only zinc and iron are selected as major elements of interest in the laser welding of DP980 steel. A flowchart representing the experimental procedure is presented in Fig. 2. The coupons are cut by an abrasive water jet machine at the required size of 300 mm in length and 50 mm in width. Then, the coupons are clamped into the fixture. The robot is programmed to follow the designated motion trajectory at a given welding speed. The CCD camera and spectrometer are also attached to the robotic arm to simultaneously capture the optical image of the weld pool and spectrum irradiated from the plasma zone and weld

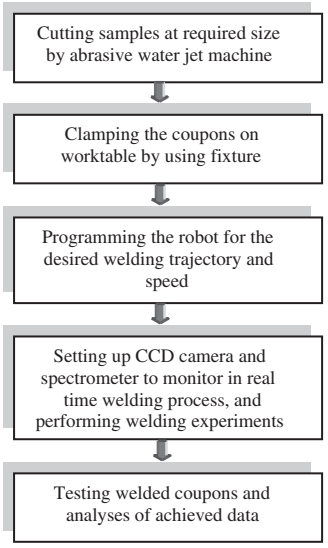

Fig. 2. Flowchart of experimental procedure of laser welding of lap jointed galvanized steel with real-time monitoring.

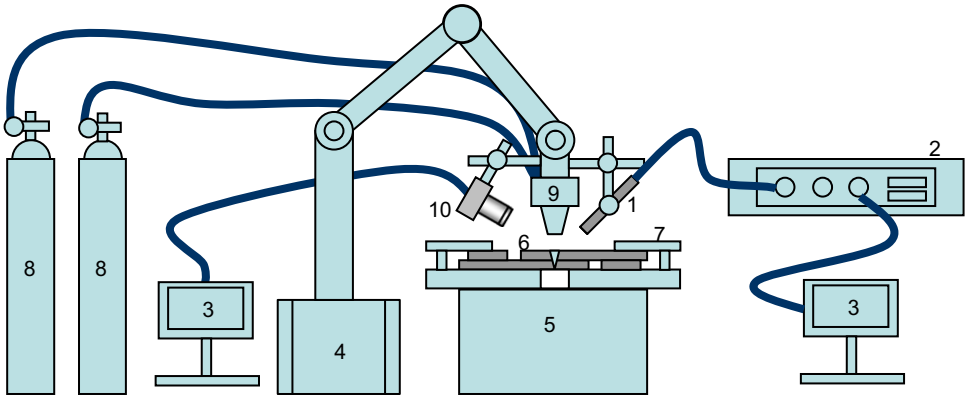

Fig. 1. Schematic of robot-controlled laser welding equipment with a spectrometer and a CCD camera monitoring system (1-colimator lens, 2-spectrometer, 3-computer, 4-robot control system, 5-worktable, 6-specimen, 7-clamp, 8-shielding gas cylinders, 9-laser welding head, and 10-CCD camera).

Table 1
Chemical compositions of galvanized DP980 steel, wt% [18,19].

C, (wt%)	Mn, (wt%)	P, (wt%)	S, (wt%)	Si, (wt%)	Cr, (wt%)	Mo, (wt%)	Al, (wt%)	Cu, (wt%)	Ni, (wt%)	Fe, (wt%)	Zn, (g/m^2)
0.15	1.5	0.014	0.006	0.31	0.02	0.01	0.05	0.02	0.01	Balance	**45**

Table 2
Design of experiments.

No.	Welding speed, (mm/s)	Laser power, (kW)	Zinc coatings at the faying interface	Thickness ratio of the top sheet to the bottom one, (mm/mm)
1	30	2.5	Fully removed	1.2 to 1.5
2	40	2.5	Fully removed	1.2 to 1.5
3	50	2.5	Fully removed	1.2 to 1.5
4	30	2.5	Remained	1.2 to 1.5
5	40	2.5	Remained	1.2 to 1.5
6	50	2.5	Remained	1.2 to 1.5
7	30	2.5	Locally removed	1.2 to 1.5

pool, respectively. The exposure time of the CCD camera is set at 0.5 ms. The experimental material coupon is galvanized high-strength steel DP980 whose chemical composition is listed in Table 1 [18,19]. Three levels of welding speeds in addition to running with or without zinc coatings at the faying surface of lap joints are selected in this study and compiled in Table 2.

3. Calculation of electron temperature

Plasma is produced inside the keyhole during high power laser welding. The plasma electron temperature T_e can be determined by means of the Boltzmann-plot, which is derived from the Boltzmann equation [20]:

$$\ln\left(\frac{I_m\lambda_m}{A_m g_m}\right) = \ln\left(\frac{hcN}{Z}\right) - \frac{E_m}{kT_e} \tag{1}$$

where E_m is the upper level energy, g_m is the statistical weight, A_m is the transition probability, λ_m the wavelength, I_m is the emission line relative intensity, k is the Boltzmann constant, h is Planck's constant, c is the light velocity, N is the total population density of the element, and Z is the partition function. Eq. (1) can be applied when the plasma plume is in local thermal equilibrium (LTE) state, which should satisfy a condition as follows [20]:

$$N_e \geq 1.6 \times 10^{12} T_e^{1/2} (\Delta E)^3 \tag{2}$$

where N_e is the electron density, and ΔE is the largest energy gap in the atomic level system.

The representation of the left-hand side of Eq. (1) versus E_m has a slope inversely proportional to T_e. Several emission lines from the same species are considered in this case to obtain the T_e profile, but this can be simplified by choosing only two lines and using Eq. (3) [21]:

$$T_e = \frac{E_m(2) - E_m(1)}{k \ln\left[\frac{E_m(1) I(1) A_m(2) g_m(2) \lambda_m(1)}{E_m(2) I(2) A_m(1) g_m(1) \lambda_m(2)}\right]} \tag{3}$$

Eq. (3) is commonly employed for on-line monitoring of welding induced plasma plume as well as weld pool, because of the reduced computational cost. Though with some loss of accuracy as compared to integrating over the entire spectrum; however, this approach is sufficient for the purpose of this study. It is worth mentioning that the obtained temperature profiles could be noisy. Also, the selection of emission lines must satisfy a condition on the upper energy levels $E_m(1)$ and $E_m(2)$ for the wavelengths $\lambda_m(1)$ and $\lambda_m(2)$, expressed by $E_m(2)–E_m(1) > kT_e$ [22]. Based on this requirement, the emission lines listed in Table 3 were selected. Table 3 lists the spectroscopic constants of Zn and Fe transitions used for the calculations, which are referenced from Ref. [23].

Table 3
Spectroscopic constants of zinc and iron transitions selected for the calculation of electron temperature [23].

Selected emission line	Wavelength, λ_m (nm)	Energy of the upper level, E_m (eV)	Statistical weight, g_m	Transition probability, A_m (s^{-1})
Zn III	382.44	32.86	4	0.4e8
Zn III	610.35	29.39	5	0.474e8
Fe I	382.85	6.87	5	1.1e8
Fe I	526.66	4.37	9	0.088e8

4. Experimental results and discussion

A CCD camera combined with green laser as an illumination source is used to monitor the dynamics of the keyhole in the weld pool. The effect of zinc coating at the interface of lap-jointed galvanized DP980 steel is experimentally studied. Fig. 3 presents captured images of the weld pool during laser welding at a power of 2.5 kW and welding speed of 30 mm/s for the experimental material conditions with and without zinc coating at the faying surface. The evolution of weld pool has been monitored by a high speed CCD camera installed above the top surfaces of the weld coupon. When the zinc coat is vaporized at the interface, zinc vapor will be vented out through the keyhole as well as the liquid zone of the weld pool, which typically produces strong spattering and blow-through holes. At the same time, the keyhole is not stable and is characterized by turbulent fluid flow, as shown in Fig. 3 for the case of zinc coating present at the faying surface. However, in the case when the zinc is mechanically removed along the faying surface, the molten pool with the keyhole is stable, as shown in Fig. 3 for the case when zinc coating is removed from the faying surface. In this case, no spattering is produced and a good weld quality is achieved.

Spectroscopy is used to detect the elemental composition in the laser induced plasma. The emission spectrum of the plasma zone is detected in real-time by using a spectrometer set over the top surface of the weld bead. In order to avoid interference from a green laser used as an external illumination source in monitoring the shape of the molten pool by the CCD camera, the detection of plasma emission lines by the spectrometer in the laser welding process is separated from the real-time monitoring of the weld pool dynamics by the CCD camera. It means each welding case was repeated twice, one with spectrometer and the other with the CCD camera assisted with a green laser. The spectrometer is aimed at the interface between the laser induced plasma and weld pool and set to acquire spectrum information ranging from a wavelength of 190 nm to 850 nm. The calculated temperature values using Eq. (3) represent a value averaged over the target spot and its surrounding area. The following analysis of the

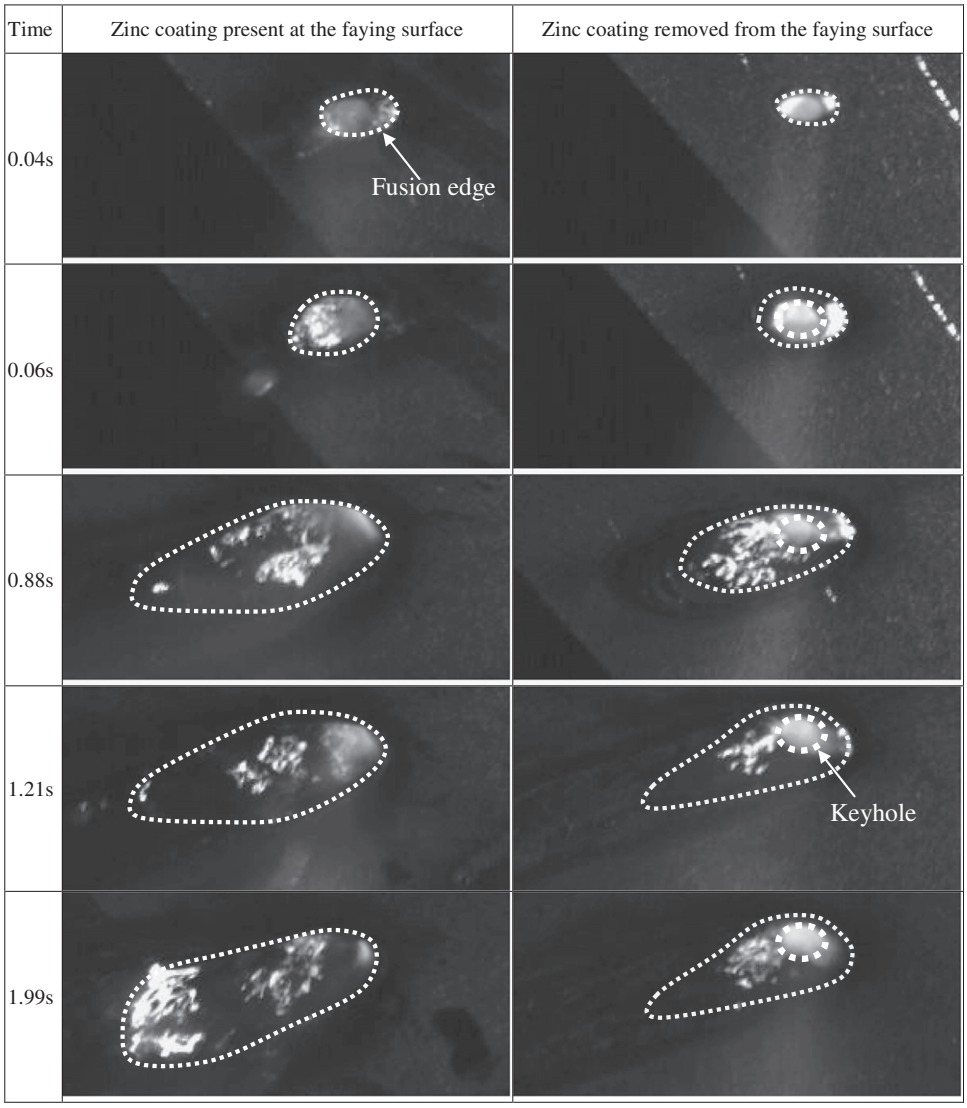

Fig. 3. Molten pool images captured by high speed CCD with green laser from the initialization of weld pool until the stable weld pool is achieved (Laser power is set at 2.5 kW, welding speed is set at 30 mm/s, an overlap joint configuration is chosen).

results exhibits a clear correlation between the changes in electron temperature with the change in behavior of the weld: good welds without zinc at the faying interface, and welds with defects for materials with zinc at the faying interface.

In order to study the influence of zinc coating at the lap joint faying surface on the intensity of emission lines in the plasma plume above the weld pool, we locally mechanically removed the zinc coating at the faying surface of lap joint as shown in Fig. 4. The coupon length is 300 mm, and the width is 50 mm. The top, bottom and cross-sectional views of laser welded overlap joints at a welding speed of 30 mm/s and a laser power of 2500 W are presented in Fig. 5. It can be seen that removing zinc at the faying surface (see Fig. 5(b)) can result in a better weld quality with respect to welds having zinc present at the faying surfaces (see Fig. 5(a)). The high pressurized zinc vapor venting out through weld pool definitely disturbs the stability of keyhole and fluid flow of the liquid phase in the weld pool, which is easily seen by real-time monitoring of CCD camera as shown in Fig. 3. Consequently, a number of spatters will be generated in the welding process due to the vaporization of zinc at the faying surface, which directly influences the stability and shape of plasma plume and corresponding intensity of featured emission lines. Fig. 6

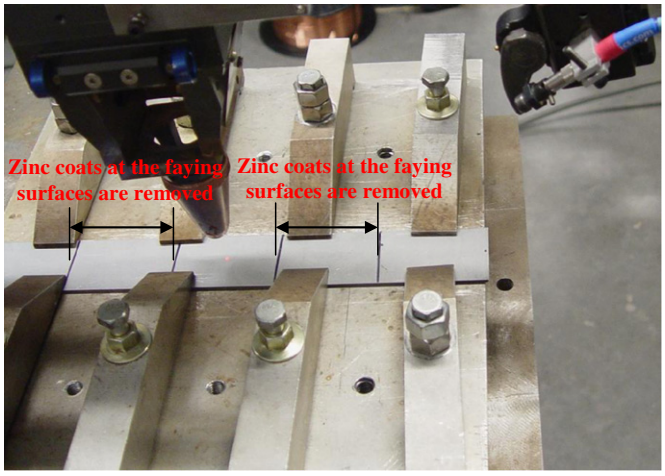

Fig. 4. Photo of spectrometer installed in the laser welding system with locally removed zinc coating from the lap joint faying surface (a) Top, bottom and cross-sectional views of lap joint with thickness of 1.2 mm-to-1.5 mm with zinc at the faying surface (b) Top, bottom and cross-sectional views of lap joint with thickness of 1.2 mm-to-1.5 mm without zinc at the faying surface.

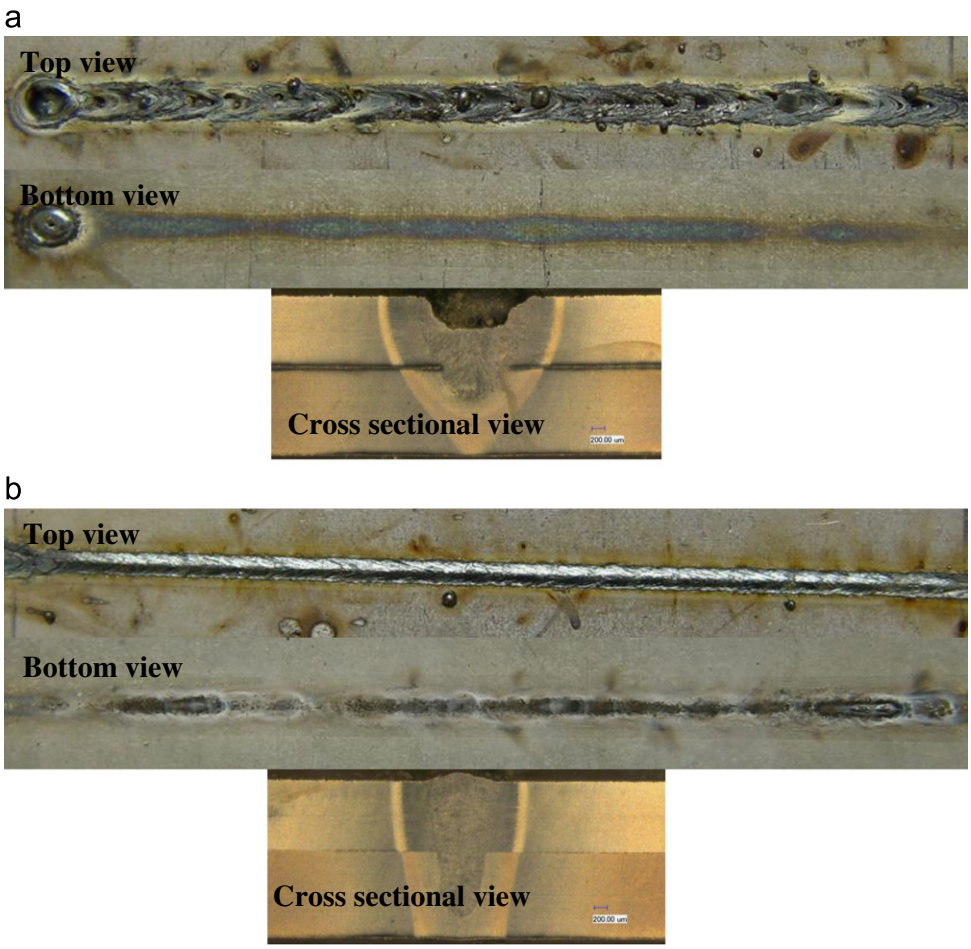

Fig. 5. Top, bottom and cross-sectional views of overlapped joints by using laser welding with a welding speed of 30 mm/s and a laser power of 2.5 kW. (a) Top, bottom and cross-sectional views of lap joint with thickness of 1.2 mm to 1.5 mm with zinc at the faying surface. (b) Top, bottom and cross-sectional views of lap joint with thickness of 1.2 mm to 1.5 mm without zinc at the faying surface.

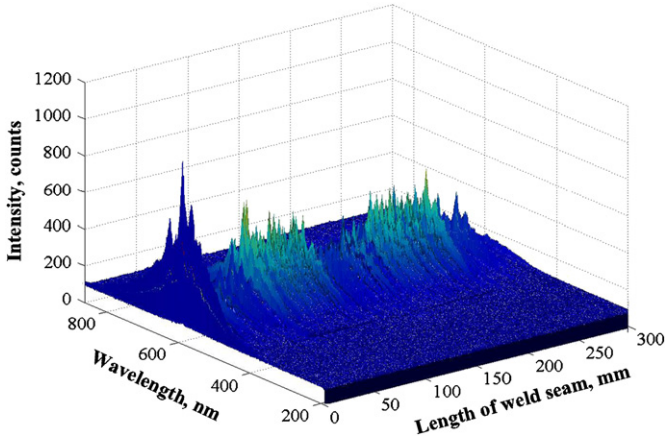

Fig. 6. Evolution of spectrum intensity in laser welding of overlapped joints with a welding speed of 30 mm/s and a laser power of 2.5 kW (thickness of sheets is 1.2 mm to 1.5 mm).

presents that evolution of spectrum intensity and Fig. 7 shows the evolution of calculated electron temperature of zinc (Fig. 7(a)) and iron (Fig. 7(b)) in laser welding of overlapped joints with a welding speed of 30 mm/s and a laser power of 2500 W, in which thickness of sheets is 1.2 mm to 1.5 mm. In general, the removal zinc at the faying surface can cause the intensity of spectrum from plasma plume to be slightly higher compared to welds having zinc present at the faying surfaces. However, the calculated electron temperature of iron and zinc when zinc is removed from the faying surface is much more uniform and lower in intensity than zinc presence at the faying surface. This should be related to the presence of the spatters caused by vaporized zinc. The presence of spatters will disturb the stability of plasma plume which causes a decrease in intensity of spectrum detected from plasma plume. However, the injection of spatters into plasma plume is supposed to increase the electron concentrations of iron and zinc elements, which is also reflected on the increase in the electron temperature of zinc and iron calculated (see Fig. 7(a) and (b)). An example of calculating the electron temperature of Fe I lines in the value of 8303 K by using the Boltzmann plot method in the case of a fiber laser welding with power of 300 W was reported in Ref. [24]. In order to verify the data presented in the cited reference, an experiment was conducted on a fiber laser welding of galvanized DP980 steel by setting the laser power at 300 W and the welding speed at 1 mm/s. The calculated average electron temperature under this condition was 7300 K. It could be concluded that there is a good qualitative agreement between these results. Based on this performed verification, the calculated electron temperatures during welding with the fiber laser of 2.5 kW in power are of reasonable values.

In order to further study the influence of welding speed on weld quality and intensity of emission lines emitted from the plasma plume during the laser welding of galvanized DP980 steel in a lap joint configuration, a series of experiments has been performed, in which coupons of 75 mm in length and 50 mm in

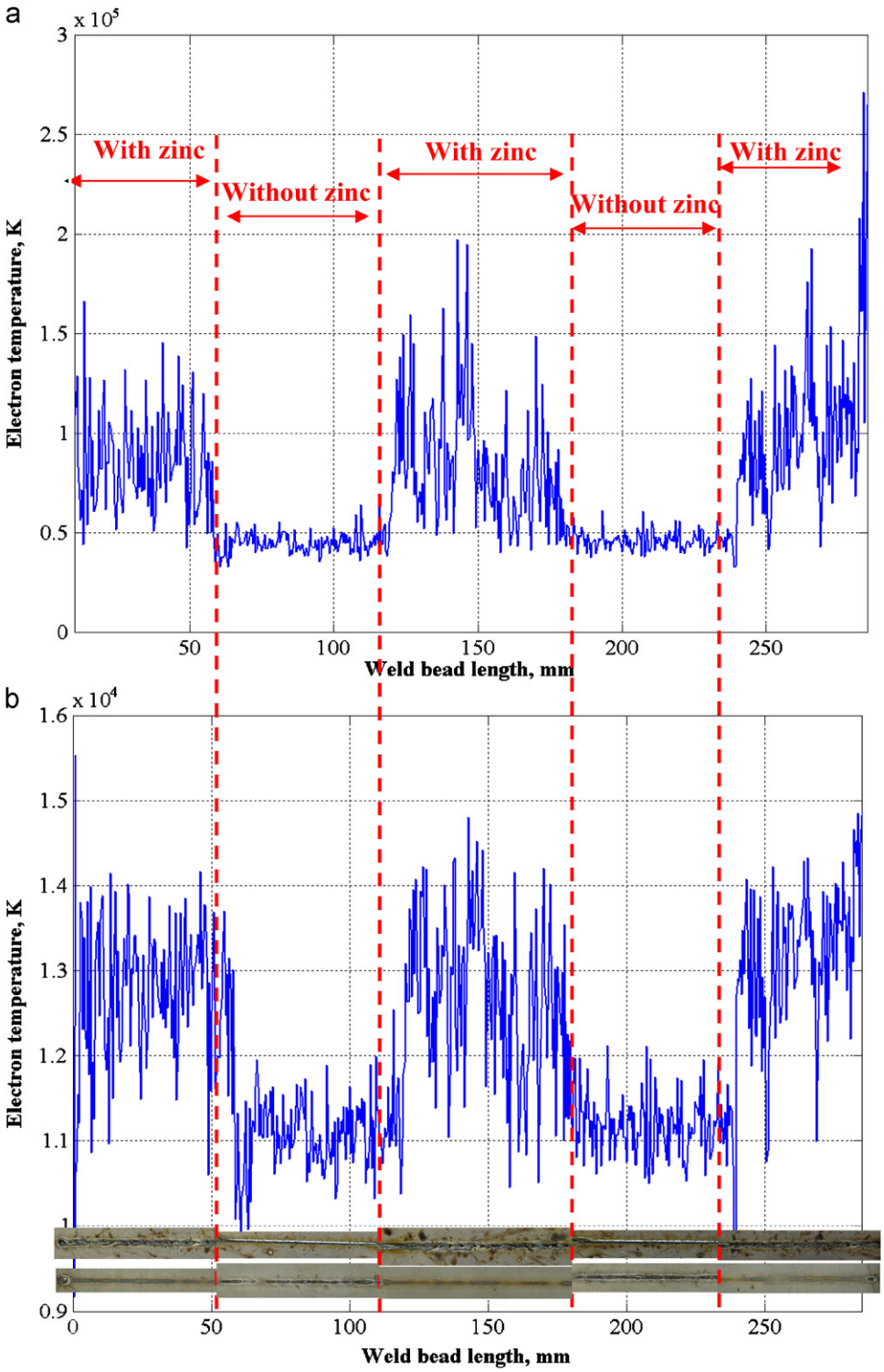

Fig. 7. Evolution of calculated electron temperature of (a) zinc and (b) iron in overlapped joints by using laser welding with a welding speed of 30 mm/s and a laser power of 2.5 kW (thickness of sheets is 1.2 mm to 1.5 mm).

width were chosen. Fig. 8(a) through c show the spectrum of laser induced plasma captured by the spectrometer without zinc coating at the faying surface of galvanized steel in a lap joint configuration, where the laser power is set at 2.5 kW, welding speed is set at 30 mm/s, 40 mm/s, and 50 mm/s, respectively. Fig. 10 presents the spectrum line distribution with wavelength obtained from the middle of the weld seam without zinc coating at the faying surface of lap-jointed galvanized steel, where the laser power was set at 2.5 kW, and welding speed was set at 50 mm/s, and the detected elements are listed in Table 4. Fig. 9(a) through c show the spectrum of laser induced plasma captured by the spectrometer with zinc coating at the faying surface of lap-jointed galvanized steel, where the laser power was set at 2.5 kW, and welding speed at 30 mm/s, 40 mm/s, and 50 mm/s, respectively. The intensity of emission lines of plasma above the weld pool is lower when the zinc coating at the faying surface is

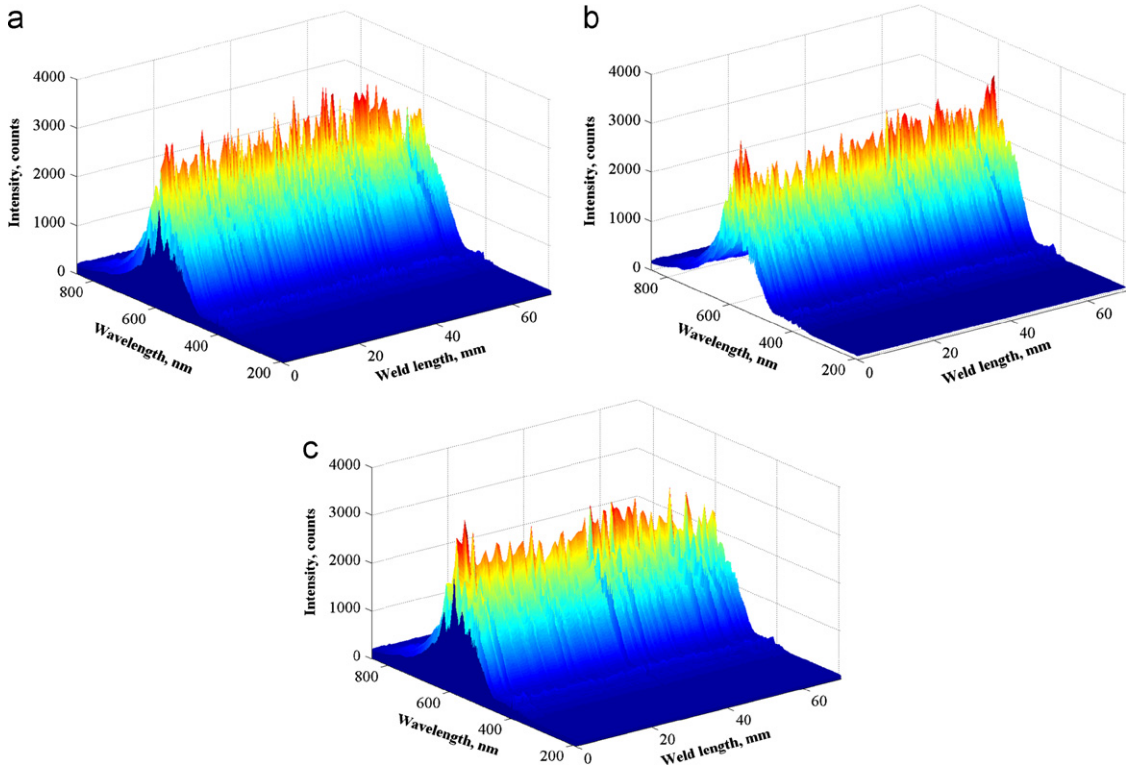

Fig. 8. Spectrum of laser induced plasma captured by spectroscopy without zinc coating at the faying surface of lap-jointed galvanized steel (laser power is set at 2.5 kW, welding speed is set at (a)30 mm/s, (b) 40 mm/s, and (c) 50 mm/s, respectively).

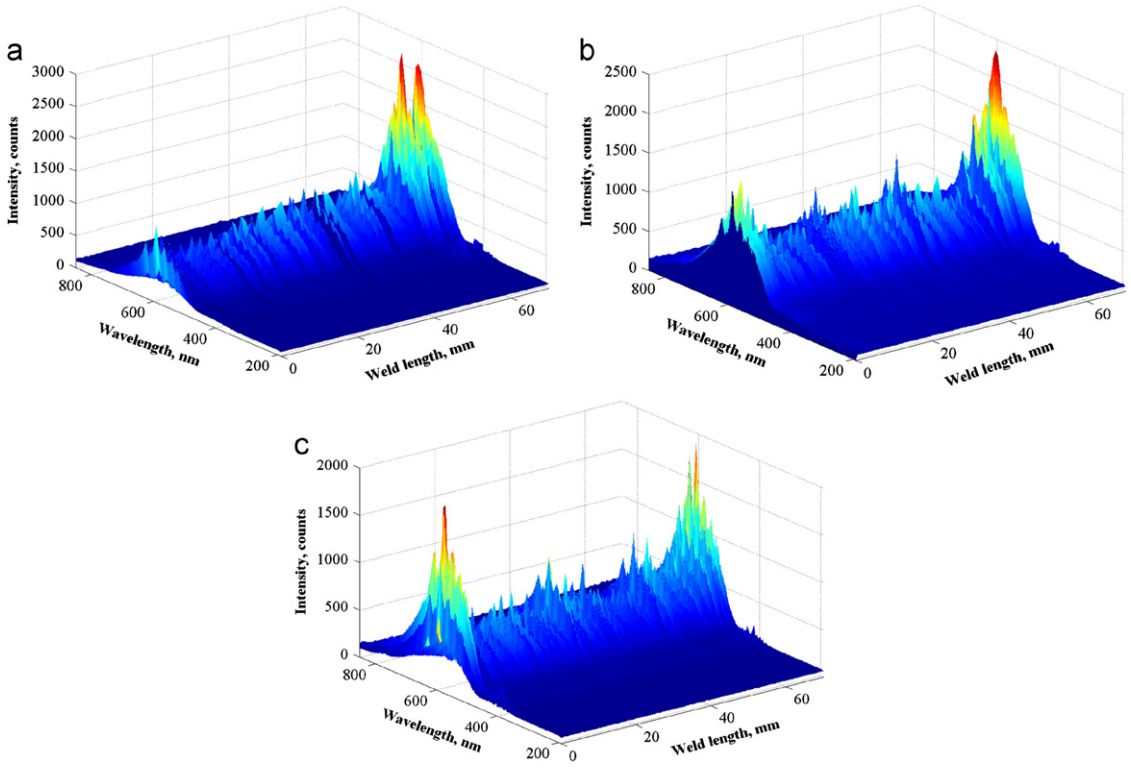

Fig. 9. Spectrum of laser induced plasma captured by spectroscopy with remained zinc coating at the faying surface of lap-jointed galvanized steel (Laser power is set at 2.5 kW, welding speed is set at (a) 30 mm/s, (b) 40 mm/s, and (c) 50 mm/s, respectively).

present. An increase in welding speed causes a slight decrease of emission line intensity from the plasma spectrum. This is because that increasing of welding speed causes the line energy density of laser power absorbed by material to decrease, which makes the light intensity of laser induced plasma plume be reduced accordingly. Fig. 11 presents a spectrum line distribution as a function of

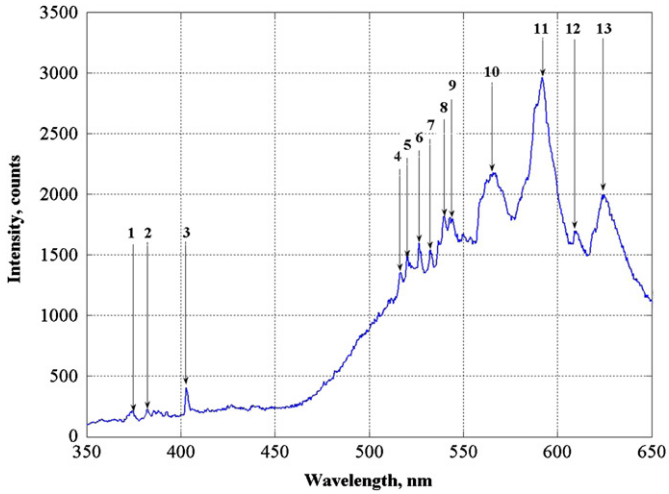

Fig. 10. Spectrum line obtained at the middle of weld bead without zinc coating at the faying surface of lap-jointed galvanized steel (laser power is set at 2.5 kW, and welding speed is set at 50 mm/s).

Table 4
Detected elements from spectrum line obtained at the middle of weld seam without zinc coating at the faying surface of lap-jointed galvanized steel shown in Fig. 10.

No. of spectrum line detected	Wavelength, (nm)	Elements detected
1	374.525	Fe, Zn
2	382.157	Fe
3	402.904	Fe
4	516.418	Fe
5	520.095	Fe
6	526.769	Fe
7	532.431	Fe
8	539.742	Fe
9	543.723	Fe
10	565.196	Fe
11	592.059	Fe
12	608.959	Fe
13	624.786	Fe

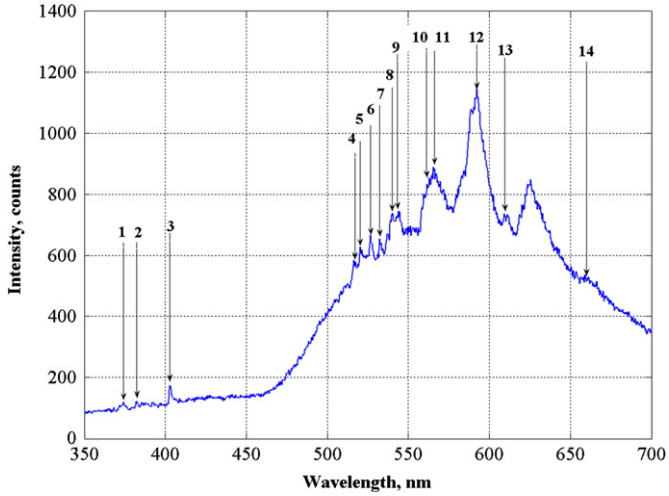

Fig. 11. Spectrum line obtained at the middle of weld bead with zinc coating at the faying surface of lap-jointed galvanized steel (laser power is set at 2.5 kW, and welding speed is set at 50 mm/s).

Table 5
Detected elements from spectrum line obtained at the middle of weld bead with zinc coating at the faying surface of lap-jointed galvanized steel shown in Fig. 11.

No. of spectrum line detected	Wavelength, (nm)	Elements detected
1	374.525	Fe, Zn
2	382.504	Fe, Zn
3	403.249	Fe, Zn
4	517.421	Fe
5	520.095	Fe
6	526.435	Fe
7	532.431	Fe
8	540.074	Fe, Zn
9	543.06	Fe
10	561.903	Fe, Zn
11	566.183	Fe
12	591.733	Fe
13	609.607	Fe
14	659.322	Fe

wavelength obtained from the middle of the weld bead with zinc coating at the faying surface of lap-jointed galvanized steel, where the laser power was set at 2.5 kW, welding speed at 50 mm/s, and the detected elements are listed in Table 5. More zinc emission lines can be detected by spectrometer from the laser plasma in the case when zinc coating is present at the faying surface, with respect to the case when zinc is removed from the faying surface (see Table 4).

Fig. 12(a) and (b) present the laser induced plasma electron temperature of iron and zinc ions, respectively. These temperatures were calculated based on spectrum captured by the spectrometer, in which conditions with and without zinc at the faying surface of lap-jointed galvanized steel are considered. The laser power is set at 2.5 kW, and the welding speed is set at 30 mm/s, 40 mm/s, and 50 mm/s. Due to the generated spatters the electron temperature of iron as well as zinc ions will be higher than that without zinc coating at the faying surface, though the former average intensity of plasma spectrum is lower than the latter one. Some peak values occur in the spectrum lines which are related to the interruption of plasma zone by spatter generation in the welding process. However, the effect of weld speed on electron temperature is negligible. That is to say, the sensitivity of electron temperature on the depth of weld penetration is ignorable.

Fig. 13(a) through c show the top and bottom surfaces of weld at different welding speeds with fully removed zinc at the faying surface. It could be noticed that a sound weld is achieved when zinc at the faying surface is fully removed before welding. An increase in welding speed can reduce the penetration depth of the weld. In comparison with Fig. 13, Fig. 14(a) through c show the top and bottom surfaces of weld at different welding speeds when zinc is present at the faying surface. It can be seen that the spattering problem becomes worse when the zinc coating is present at the faying surface. Fig. 15(a) through c show micrographs of cross-sections of lap-jointed DP980 coupons with welding speeds of 30 mm/s, 40 mm/s and 50 mm/s, respectively, without zinc coatings at the faying surface. Fig. 16(a) through c show micrographs of cross-sections of lap-jointed DP980 coupons with welding speeds of 30 mm/s, 40 mm/s and 50 mm/s, respectively, with zinc coating at the faying surface. It can be summarized that the generation of spatter caused by ejection of zinc vapor from the faying surface prevents the laser beam from penetrating the weld bead resulting in a shallower penetration of weld as well as poor surface quality.

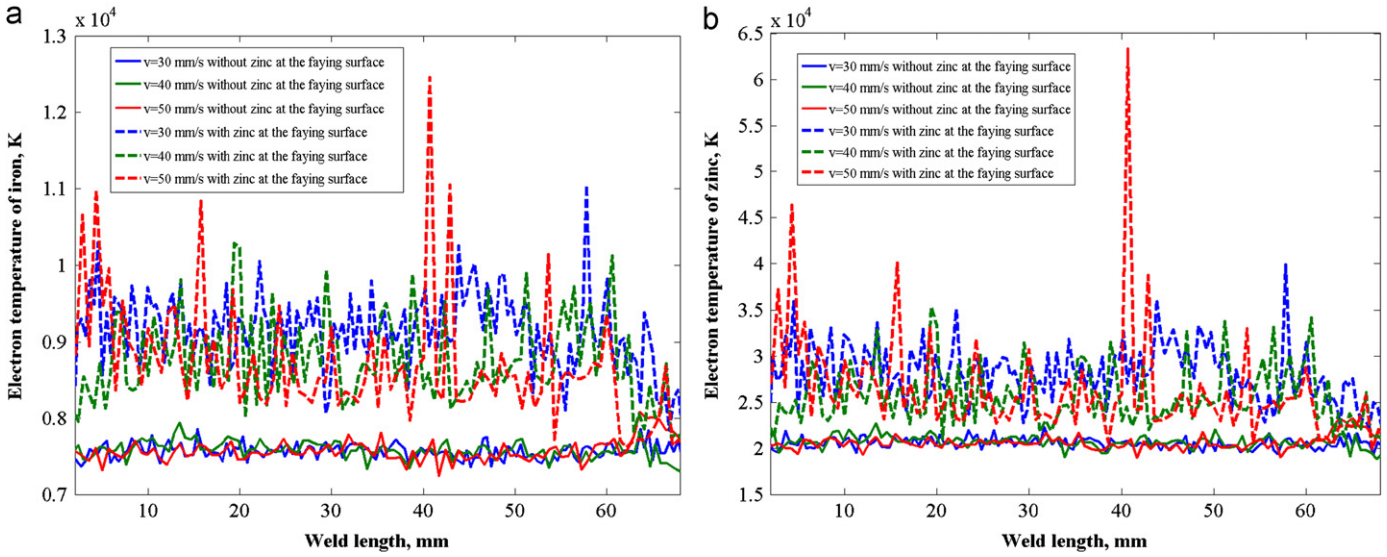

Fig. 12. Electron temperature of iron (a) and zinc (b) in laser induced plasma calculated based on spectrum captured by spectrometer with and without zinc coating at the faying surface of lap-jointed galvanized steel (laser power is set at 2.5 kW, welding speed is set at 30 mm/s, 40 mm/s, and 50 mm/s).

Fig. 13. The top and bottom views of DP980 weld obtained by laser power of 2.5 kW and fully removed zinc coating at the faying interface. (a) $v=30$ mm/s. (b) $v=40$ mm/s. (c) $v=50$ mm/s.

5. Conclusions

A series of experiments has been performed to detect the zinc vapor signals by using spectroscopy, and to monitor the weld pool dynamics by using a CCD camera assisted with a green laser as an illumination source. Based on the performed analysis, the following could be concluded:

(1) There is a good correlation between the change in the average electron temperature, acquired from the surrounding area of

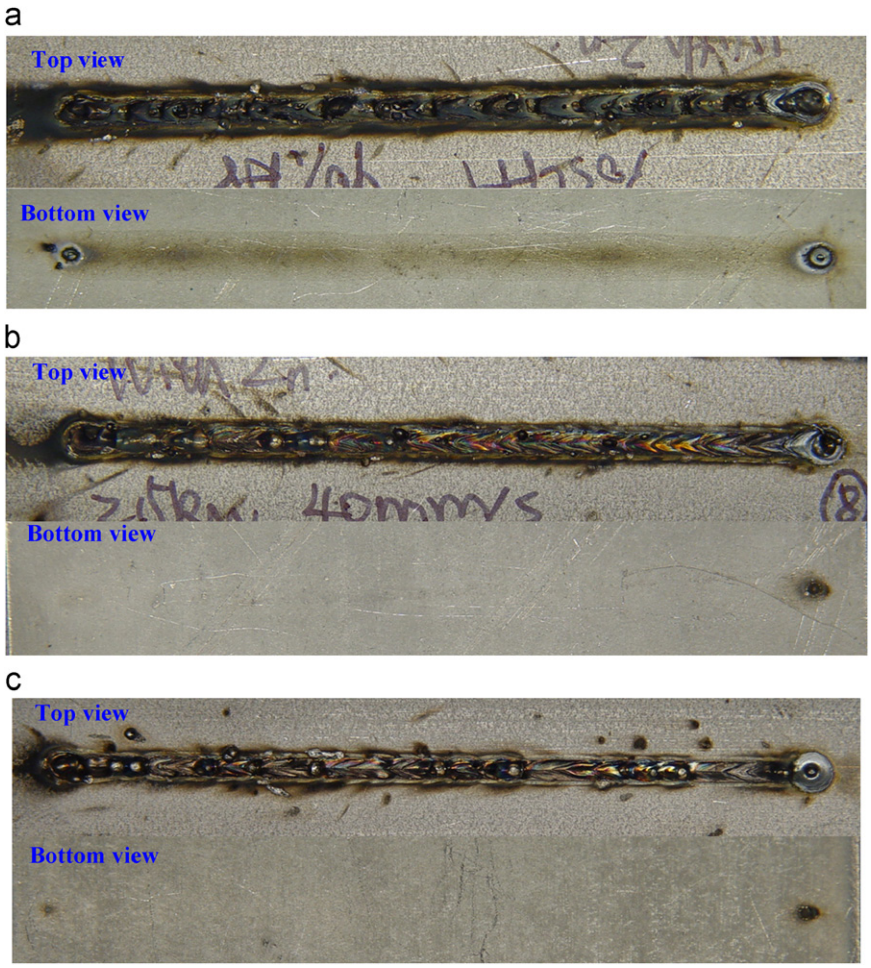

Fig. 14. The top and bottom views of DP980 weld obtained by laser power of 2.5 kW and zinc coating at the faying interface remained. (a) $v=30$ mm/s, (b) $v=40$ mm/s, and (c) $v=50$ mm/s.

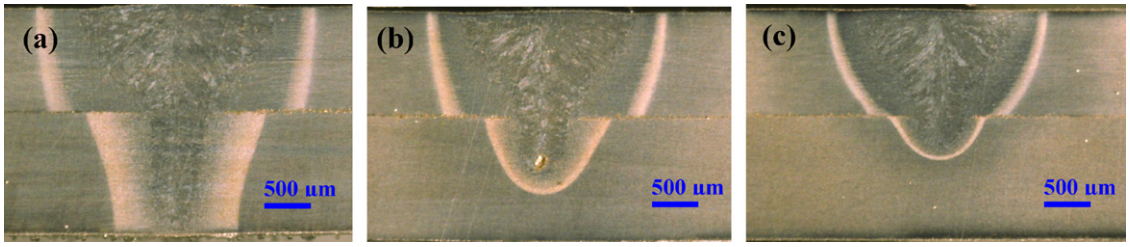

Fig. 15. The cross-sectional views of DP980 weld obtained by laser power of 2.5 kW and fully removed zinc coating at the faying interface (a) $v=30$ mm/s, (b) $v=40$ mm/s, and (c) $v=50$ mm/s.

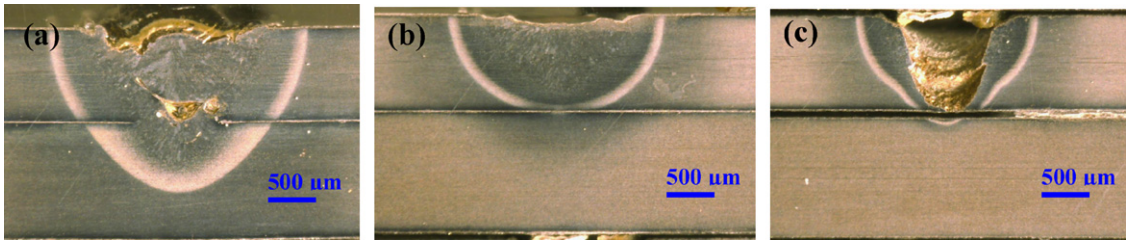

Fig. 16. The cross-sectional views of DP980 weld obtained by laser power of 2.5 kW and remained zinc coating at the faying interface (a) $v=30$ mm/s, (b) $v=40$ mm/s, and (c) $v=50$ mm/s.

the laser-weld pool interface, and the remained weld defects like spatters during laser welding process. However, the sensitivity of electron temperature on the depth of weld penetration is negligible.

(2) The keyhole dynamic behavior as well as liquid flow in the molten pool depends directly on the behavior of zinc vapor at the faying surface, which can be clearly monitored by a high frame rate CCD camera.

(3) An increase in welding speed can cause a slight reduction in the plasma spectrum intensity and will decrease the depth of weld penetration.
(4) The depth of weld penetration will increase if the zinc coating is removed.

Acknowledgement

The authors would like to thank research engineer, Mr. Andrew Socha at the Research Center for Advanced Manufacturing, Southern Methodist University for his design of clamping tool and maintenance of experimental equipment. This work was financially supported by NSF's Grant No. IIP-1034652.

References

[1] Akhter R, Steen WM, Watkins KG. Welding zinc-coated steel with a laser and the properties of the weldment. Journal of Laser Applications 1991;3(2): 9–20.
[2] Li XG, Lawson WHS, Zhou YN. Lap welding of steel articles having a corrosion resisting metallic coating. U.S. Patent 2008/0035615 A1, 2008.
[3] Mazumder J, Dasgupta A, Bembenek M. 2002. Alloy based laser welding. U.S. Patent 6,479,168.
[4] Gualini MMS, Iqbal S, Grassi F. Modified dual-beam method for welding galvanized steel sheets in lap configuration. Journal of Laser Applications 2006;18(3):185–91.
[5] Yang SL, Kovacevic R. Welding of galvanized dual-phase 980 steel in a gap-free lap joint configuration. Welding Journal 2009;88(8):168–78.
[6] Sibillano T, Ancona A, Berardi V, Lugarà PM. A real-time spectroscopic sensor for monitoring laser welding processes. Sensors 2009;9:3376–85.
[7] Fabbro R, Coste F, Goebels D, Kielwasser M. Study of CW Nd-YAG laser welding of Zn-coated steel sheets. Journal of Physics D: Applied Physics 2006;39:401–9.
[8] Park YW, Park H, Rhee S, Munjin K. Real-time estimation of CO_2 laser weld quality for automotive industry. Optics & Laser Technology 2002;34:135–42.
[9] Park H, Rhee S. Analysis of mechanism of plasma and spatter in CO_2 laser welding of galvanized steel. Optics & Laser Technology 1999;31(2):119–26.
[10] Bruncko J, Uherek F, Michalka M. Monitoring of laser welding by optical emission spectroscopy. Laser Physics 2003;13(4):669–73.
[11] Rodil SS, Gómez RA, Bernárdez JM, Rodríguez F, Miguel LJ, Perán JR. Laser welding defects detection in automotive industry based on radiation and spectroscopical measurements. International Journal of Advanced Manufacturing Technology 2010;49:133–45.
[12] Mirapeix J, Cobo A, Fernandez S, Cardoso R, Lopez-Higuera JM. Spectroscopic analysis of the plasma continuum radiation for on-line arc-welding defect detection. Journal of Physics D: Applied Physics 2006;41:135202–10.
[13] Ancona A, Lugarà PM, Ottonelli F, Catalano IM. A sensing torch for on-line monitoring of the gas tungsten arc welding process of steel pipes. Measurement Science and Technology 2004;15:2412–8.
[14] Sadek CAA, Diogo DSM, Marcelo SM. Emission spectrometry evaluation in arc welding monitoring system. Journal of Materials Processing Technology 2006;179:219–24.
[15] Kato B, Furuzawa H, Morita K, Isono E. Identification of weld defects by ultrasonic spectroscopy. Transactions of the Japan Welding Society 1971;2(2): 71–80.
[16] Li ZY, Wang B, Ding JB. Detection of GTA welding quality and disturbance factors with spectral signal of arc light. Journal of Materials Processing Technology 2009;209:4867–73.
[17] García-Allende PB, Mirapeix J, Conde OM, Cobo A, Lpez-Higuera JM. Spectral processing technique based on feature selection and artificial neural networks for arc welding quality monitoring. NDT&E International 2009;42: 56–63.
[18] Xia MS, Biro E, Tian ZL, Norman Zhou Y. Effects of heat input and martensite on HAZ softening in laser welding of dual phase steels. ISIJ International 2008;48(6):809–14.
[19] Burns Trevor J. Weldability of a dual-phase sheet steel by the gas metal arc welding process. Master Thesis, The University of Waterloo, 2009.
[20] Griem HR. Principle of Plasma Spectroscopy. Cambridge Monographs on Plasma Physics. Cambridge: Cambridge University Press; 1997.
[21] Marotta A. Determination of axial thermal plasma temperatures without Abel inversion. Journal of Physics D: Applied Physics 1994;27:268–72.
[22] Lacroix D, Jeandel G, Boudot C. Spectroscopic characterization of laser-induced plasma created during welding with a pulsed Nd: YAG laser. Journal of Physics D: Applied Physics 1997;81(10):6599–606.
[23] Wiese WL, Martin GA. Wavelengths and transition probabilities for atoms and atomic ions. Part II. Transition Probability 1980:378–406.
[24] Alexander Grant Paleocrassas. Process characterization of low speed, fiber laser welding of AA 7075-T6 application to fatigue crack repair. Ph.D. Dissertation, North Carolina State University, 2009.